

Resolution scaling in STED microscopy

Benjamin Harke, Jan Keller, Chaitanya K. Ullal, Volker Westphal,
Andreas Schönle and Stefan W. Hell*

Max Planck Institute for Biophysical Chemistry, Am Fassberg 11, 37077 Göttingen, Germany

*Corresponding author: shell@gwdg.de

Abstract: We undertake a comprehensive study of the inverse square root dependence of spatial resolution on the saturation factor in stimulated emission depletion (STED) microscopy and generalize it to account for various focal depletion patterns. We used an experimental platform featuring a high quality depletion pattern which results in operation close to the optimal optical performance. Its superior image brightness and uniform effective resolution <25 nm are evidenced by imaging both isolated and self-organized convectively assembled fluorescent beads. For relevant saturation values, the generalized square-root law is shown to predict the practical resolution with high accuracy.

©2008 Optical Society of America

OCIS codes: (180.2520) Microscopy : Fluorescence microscopy; (180.4315) Microscopy : Nonlinear microscopy; (220.1230) Optical design and fabrication : Apodization; (350.3730) Other areas of optics : Resolution.

References and links

1. S. G. Megason and S. E. Fraser, "Imaging in systems biology," *Cell* **130**, 784-795 (2007).
2. S. W. Hell, "Far-Field Optical Nanoscopy," *Science* **316**, 1153-1158 (2007).
3. W. E. Moerner, "New directions in single-molecule imaging and analysis," *Proc. Natl. Acad. Sci. U. S. A.* **104**, 12596-12602 (2007).
4. A. Heinrichs, "Imaging: Overcoming the barrier," *Nat. Rev. Mol. Cell Biol.* **7**, 707-707 (2006).
5. S. W. Hell and J. Wichmann, "Breaking the diffraction resolution limit by stimulated emission: stimulated emission depletion microscopy," *Opt. Lett.* **19**, 780-782 (1994).
6. T. A. Klar and S. W. Hell, "Subdiffraction resolution in far-field fluorescence microscopy," *Opt. Lett.* **24**, 954-956 (1999).
7. M. Dyba and S. W. Hell, "Focal spots of size $1/23$ open up far-field fluorescence microscopy at 33 nm axial resolution," *Phys. Rev. Lett.* **88**, 163901 (2002).
8. E. Betzig, G. H. Patterson, R. Sougrat, O. W. Lindwasser, S. Olenych, J. S. Bonifacino, M. W. Davidson, J. Lippincott-Schwartz, and H. F. Hess, "Imaging Intracellular Fluorescent Proteins at Nanometer Resolution," *Science* **313**, 1642-1645 (2006).
9. S. T. Hess, T. P. K. Girirajan, and M. D. Mason, "Ultra-High Resolution Imaging by Fluorescence Photoactivation Localization Microscopy," *Biophys. J.* **91**, 4258-4272 (2006).
10. M. J. Rust, M. Bates, and X. Zhuang, "Sub-diffraction-limit imaging by stochastic optical reconstruction microscopy (STORM)," *Nature Methods* **3**, 793-796 (2006).
11. A. Sharonov and R. M. Hochstrasser, "Wide-field subdiffraction imaging by accumulated binding of diffusing probes," *Proc. Natl. Acad. Sci. U. S. A.* **103**, 18911-18916 (2006).
12. M. Hofmann, C. Eggeling, S. Jakobs, and S. W. Hell "Breaking the diffraction barrier in fluorescence microscopy at low light intensities by using reversibly photoswitchable proteins," *Proc. Natl. Acad. Sci. U. S. A.* **102**, 17565-17569 (2005).
13. M. G. L. Gustafsson, "Nonlinear structured-illumination microscopy: Wide-field fluorescence imaging with theoretically unlimited resolution," *Proc. Natl. Acad. Sci. U. S. A.* **102**, 13081-13086 (2005).
14. K. I. Willig, S. O. Rizzoli, V. Westphal, R. Jahn, and S. W. Hell, "STED-microscopy reveals that synaptotagmin remains clustered after synaptic vesicle exocytosis.," *Nature* **440**, 935-939 (2006).
15. R. J. Kittel, C. Wichmann, T. M. Rasse, W. Fouquet, M. Schmidt, A. Schmid, D. A. Wagh, C. Pawlu, R. Kellner, K. I. Willig, S. W. Hell, E. Buchner, M. Heckmann, and S. J. Sigrist, "Bruchpilot Promotes Active Zone Assembly, Ca²⁺-Channel Clustering, and Vesicle Release," *Science* **312**, 1051-1054 (2006).
16. J. J. Sieber, K. I. Willig, C. Kutzner, C. Gerding-Reimers, B. Harke, G. Donnert, B. Rammner, C. Eggeling, S. W. Hell, H. Grubmüller, and T. Lang, "Anatomy and dynamics of a supramolecular membrane protein cluster," *Science* **317**, 1072 - 1076 (2007).
17. B. Harke, C. K. Ullal, J. Keller, and S. W. Hell, "Three-Dimensional Nanoscopy of Colloidal Crystals," *Nano. Lett. ASAP Article* 10.1021/nl073164n (2008).
18. J. Keller, A. Schönle, and S. W. Hell, "Efficient fluorescence inhibition patterns for RESOLFT microscopy," *Opt. Express* **15**, 3361-3371 (2007).
19. S. W. Hell, "Toward fluorescence nanoscopy," *Nat. Biotechnol.* **21**, 1347-1355 (2003).

20. V. Westphal and S. W. Hell, "Nanoscale Resolution in the Focal Plane of an Optical Microscope," *Phys. Rev. Lett.* **94**, 143903 (2005).
21. M. Dyba, J. Keller, and S. W. Hell, "Phase filter enhanced STED-4Pi fluorescence microscopy: theory and experiment," *New J. Phys.* **7** (2005).
22. K. I. Willig, B. Harke, R. Medda, and S. W. Hell, "STED microscopy with continuous wave beams," *Nature Methods* **4**, 915-918 (2007).
23. K. Willig, J. Keller, M. Bossi, and S. W. Hell, "STED microscopy resolves nanoparticle assemblies," *New J. Phys.* **8**, 106 (2006).
24. N. D. Denkov, O. D. Velev, P. A. Kralchevsky, I. B. Ivanov, H. Yoshimura, and K. Nagayama, "Mechanism of Formation of 2-Dimensional Crystals from Latex-Particles on Substrates," *Langmuir* **8**, 3183-3190 (1992).
25. V. Westphal, C. M. Blanca, M. Dyba, L. Kastrop, and S. W. Hell, "Laser-diode-stimulated emission depletion microscopy," *Appl. Phys. Lett.* **82**, 3125-3127 (2003).

1. Introduction

The ability of far field fluorescence microscopy to image with a resolution far beyond the diffraction limit has been the subject of considerable recent interest [1-4]. In particular, the demonstration of resolutions down to a few tens of nanometers in STED (Stimulated Emission Depletion) microscopy has marked the advent of far-field optical nanoscopy [5-7]. A clutch of techniques that exploit the spectral properties of fluorophores, specifically a selected pair of dark and bright states, to achieve such resolutions have since been demonstrated [8-13]. At the same time, STED has been applied to a multitude of imaging tasks [14-17] mainly in biology and more recently, STED microscopes have become commercially available. The resolution achieved by such a far-field optical microscope is no longer fundamentally limited by the wave nature of light but rather, depends only on the available laser power and the quality of the implementation. Here we validate a simple formula predicting the resolution of a STED microscope at given experimental parameters and demonstrate that this theoretical mark can indeed be reached by a standard implementation using readily available optical components.

In the STED microscope the diffraction limited excitation focus is overlaid with a red shifted STED beam featuring a zero intensity point. The STED beam depletes the molecular fluorescent state everywhere within the focal region by means of stimulated emission, except at the zero intensity point and its proximity, thereby confining the spatial extent of effective molecular excitation and hence of fluorescence. The depletion is driven by de-excitation through stimulated emission and the saturation of this transition provides the non-linear response that allows for the manipulation of the shape and size of the effective fluorescent spot beyond the diffraction limit. The resolution of the STED microscope is thus a function of the spatial distribution and magnitude of the intensity of the depleting light, with no theoretical limit to the ultimate achievable value. Nonetheless, the nature and factual quality of the focal intensity patterns of the STED beam strongly impacts the resolution achieved by a particular configuration. Typically, a doughnut shaped distribution is targeted so as to obtain the most uniform resolution increase in the focal plane. Systematic studies based on the vectorial analysis of image formation have suggested the use of a phase mask designed to impart a helical phase retardation to the STED beam, in order to obtain the optimal inhibition pattern for enhancement of the resolution in the focal plane [18]. In addition, it was shown that a phase mask with a phase retardation of π over a central circular area yielded optimum confinement of the fluorescence mainly along the axial direction. Prior to this, the dependence of the resolution on the applied intensity of the STED beam had been modeled, and was shown to increase with the inverse square root of the saturation level [19]. An initial experimental confirmation of the square root behaviour was provided by imaging single molecules with a STED configuration that possessed resolution enhancement in one principal direction [20]. However, the polarisation dependence inherent in the scheme used yielded a dispersion of the measured sizes of the effective focal spots. The application of linear excitation, depletion as well as detection when coupled with the random but fixed orientations of the isolated single molecules resulted in different cross sections for the depletion mechanism. This non-uniformity manifested itself as variability in the resolution evidenced for specific powers.

In this paper, a high precision and comprehensive validation of the square root law is presented. The theoretical derivation is generalized to account for variations in the form of the depletion patterns and the new expression yields quantitative predictions of the achievable resolution. It is validated experimentally, for both lateral and axial confinements. To this end, a simplified STED configuration is applied in an ensemble measurement of 24 nm beads filled with dye molecules, thereby eliminating the previously mentioned variability introduced by the random orientation, blinking and bleaching of isolated single molecules. Several performance enhancements demonstrated by this improved setup are quantitatively established. These include obtaining a high quality depletion pattern with an associated increase in brightness of acquired images and delivering a uniform effective resolution in the lateral directions of the focal plane. The enhanced performance is demonstrated by imaging self organized convectively assembled 200 nm fluorescent beads.

2. Theory

The approximate functional dependence of resolution increase expected in a STED microscope on the intensity of the depletion light has been derived [19, 20]. The FWHM of the resulting spot has been shown to depend on the inverse square root of the saturation factor

$$\Delta x \propto \lambda / n \sqrt{\zeta} \quad (1)$$

where λ is the inhibition wavelength, n is the refractive index and ζ denotes the saturation factor which is defined as:

$$\zeta = I_{STED} / I_s \quad (2)$$

I_{STED} is the maximum of the intensity distribution of the inhibition light and I_s is the effective saturation intensity which can be defined as the intensity at which the probability of fluorescence emission is reduced by half. In the most general case, I_s is a function of the orientational distribution and rotational behavior of the dye molecules, as well as the wavelength, temporal structure, and polarization of the inhibition light.

We follow a similar derivation as in [20] extending and generalizing it to accommodate the particularities of the depletion patterns actually used. We define the suppression factor $\eta(\mathbf{x})$ as the fraction of fluorescence still detected at position \mathbf{x} in the presence of inhibition light of intensity $I_{STED}(\mathbf{x})$. For temporally separated excitation and inhibition light, after averaging over the dye's orientation, the suppression factor can usually be well approximated by an exponential [21]:

$$\eta(x) \equiv \exp(-\ln(2) I_{STED}(x) / I_s) \quad (3)$$

Clearly the width of the central peak along any direction strongly depends on the shape of the focal inhibition light pattern. We choose a linear approximation for the electric field close to the focal point, and the de-excitation intensity pattern can then be approximated by a parabola with its minimum at the focal point, i.e.

$$I_{STED}(x) = 4I_{STED} a^2 x^2 \quad (4)$$

Here, x is the coordinate along a particular direction and a is the pattern steepness along this direction. An intuitive way to estimate the performance of the STED microscope is as the improvement over the resolution d_c of a confocal microscope. The confocal PSF $h_c(\mathbf{x})$ can be well described by a Gaussian in the vicinity of the focal spot. For usual pinhole sizes, its width in the focal plane is $\approx \lambda / (2NA)$ due to diffraction. $NA = n \sin \alpha$ is the numerical aperture of the objective lens given by the product of the refractive index of the medium and the sine of the half aperture angle α of the lens. The effective PSF of the STED microscope is then given by:

$$h_{eff}(\mathbf{x}) = h_c(\mathbf{x}) \eta(\mathbf{x}) \quad (5)$$

Due to the exponential behavior in Eq. (3) this is a Gaussian with a reduced width along x

$$h_{eff}(x) = \exp(-4 \ln(2) x^2 (d_c^{-2} + a^2 \zeta)) \quad (6)$$

The new FWHM along x is therefore

$$d = d_c / \sqrt{1 + d_c^2 a^2 \zeta} \quad (7)$$

The confocal width is reproduced for $\zeta = 0$. For large saturation levels on the other hand, the effective resolution of a STED microscope is governed only by the product of the pattern steepness and the square root of the saturation factor. Eq. (7) does then become independent of d_c :

$$d \cong 1 / (a \sqrt{\zeta}) \quad (8)$$

3. Setup

A schematic diagram of the setup used is shown in Fig. 1(a). An excitation wavelength of 635 nm was generated by a pulsed laser diode (Picoquant, Berlin, Germany). The pulse width was 70 ps. Each excitation pulse was directly followed by a red shifted STED pulse generated by a femtosecond modelocked Titanium Sapphire laser (MIRA900, Coherent, USA) running at a repetition rate of 76 MHz. The STED pulses of originally less than 100 fs duration were stretched to about 300 ps by guiding the light through 100 meters of single mode, polarization-maintaining fibre. In order to avoid non-linear effects in the fibre the STED pulses were pre-stretched by guiding them through 120 cm heavy flint glass (SF6) rods prior to entering the fibre. The delay between the two pulses was realized electronically by using the output signal of the photo diode of the STED laser to trigger the pulsed excitation diode. A custom-made delay unit was employed to synchronize the arrival of the two pulses within a precision of 10 ps. The STED beam that was coupled out of the single mode fibre was passed through a polymeric phase plate (vortex pattern, RPC Photonics, Rochester, NY, USA) and subsequently overlaid with the excitation beam using a dichroic mirror. The combination of a half-wave and a quarter-waveplate was used to impart a circular polarization to the STED and excitation beams. The use of circular polarization for excitation, depletion and detection yields a uniform effective resolution increase in the lateral directions of the focal plane of the objective lens (NA 1.4 Oil immersion, 100x PL APO, Leica). A spectrum of the dye used for imaging is shown in Fig. 1(b). The detection window was thus set between 650 nm and 690 nm. A strong fluorescence inhibition with a lowered probability of attendant residual excitation was targeted by setting the STED wavelength to 735 nm. The fluorescence signal was detected confocally by getting a multi mode fibre, whose diameter corresponded to 0.7 Airy discs, to serve as the confocal pinhole. The reasons for using a pinhole are the rejection of stray and ambient light and the convenient confocal axial sectioning provided by this scheme. Note that confocality is not an ingredient of the concept of STED microscopy, because for the relevant saturation factors, $h_{eff}(x)$ is dominated by the depletion function $\eta(x)$, not by the detection function of the confocal pinhole. Imaging was achieved by piezoscanning the sample on a xyz scan stage (Nanoblock, Melles Griot) and recording the fluorescence signal with a photon-counting APD (Perkin Elmer).

A key element in the setup was the utilization of a polymer phase plate that imparted a helical phase retardation to the STED beam. The phase plate, a standard optical element available from a manufacturer specializing in creating optical vortices (RPC Photonics), displays a thickness profile similar to that shown in Fig. 1(c). The profile was fabricated such that the maximal thickness of the polymer corresponded to a phase retardation of 2π for the STED wavelength employed. The incorporation of the polymer phase plate results in a compact setup. In contrast to a prior implementation of the helical phase mask using a more expensive spatial light modulator no imaging of the phase onto the back aperture of the objective lens is necessary. Further, the polymer phase plate makes accessible the use of high average powers, as is required in the case of continuous wave STED microscopy[22].

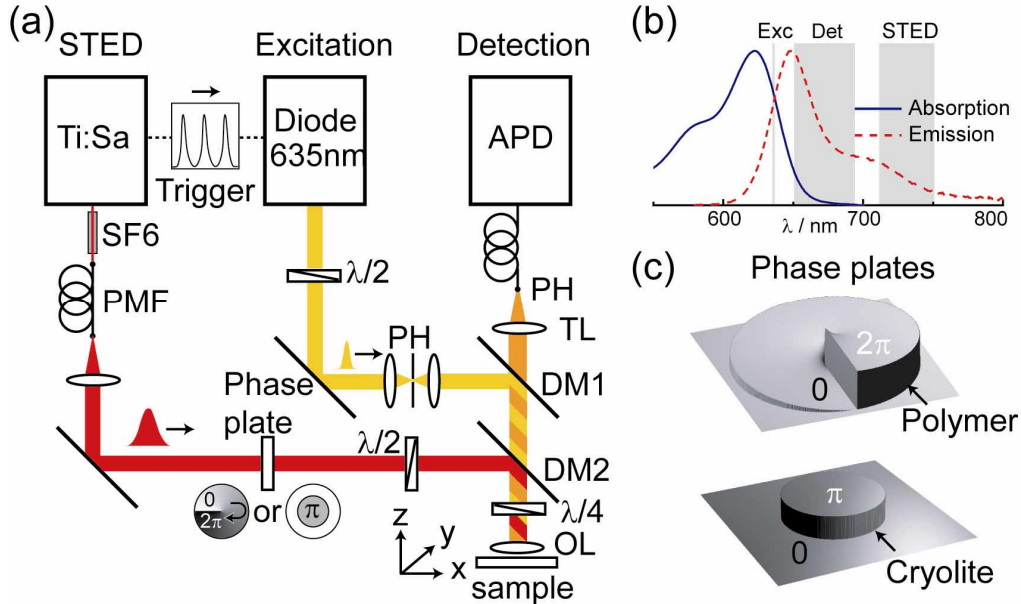


Fig. 1. Experimental platform; (a) Setup. PMF: polarisation maintaining fibre; APD: avalanche photo diode; PH: pinhole; TL: tube lens; DM: dichroic mirror; OL: objective lens; SF6: glass rods. (b) Absorption and emission spectrum of a solution of 24 nm fluorescent beads used in the presented measurements. (c) 3D view of the phase masks used for the measurements.

4. Results

To observe the impact of the improved resolution we imaged fluorescent nanospheres. Such a system displays a low incidence of photo-bleaching thereby allowing for the precise quantification of the resolution dependence on the applied STED power. A dilute dispersion of dye-filled 24 nm polystyrene beads (crimson beads, Invitrogen, USA), prepared by drop casting a solution of the beads on a Poly-L-Lysine coated glass coverslip, was imaged at different STED intensities. Mowiol (Hoechst, Germany) was used as the mounting medium. Confocal and STED images of the beads are shown in Fig. 2(a) and 2(b), respectively. The beads in the confocal image are blurred whereas nearly every individual bead can be resolved in the STED counterpart. A series of images with STED intensities corresponding to 0 MW/cm², 40 MW/cm², 158 MW/cm², 316 MW/cm² and 1.7 GW/cm², respectively, were taken. The concomitant improvement of spatial resolution in the focal plane by an order of magnitude is vividly demonstrated in the suppl. Movie 1 (avi, 2.6MB). The region indicated by the white rectangles in Fig. 2(a,b) are shown in Fig. 2(c-g) for the respective powers. The properties of the dye being interrogated were accounted for by quantifying the depletion through stimulated emission at various intensities. Figure 2(h) shows such a depletion curve measured on the same sample. To obtain a value for the saturation intensity I_S , the excitation beam and a regularly focused STED beam were overlaid in space and the fluorescence signal integrated over a scan area were compared at different STED intensities. I_S was established to ~11 MW/cm² by correcting for the spatial distributions of the corresponding PSFs.

Resolution measurements, shown in Fig. 3, were performed on a further diluted dispersion of beads. The mean bead size for each power setting was determined by measuring the FWHM of the Gaussian distribution fitted to profiles of individual beads and averaging over 20 - 30 beads. The resulting error bars are almost not visible in the presented data. Since the average size of the beads is known, determined by electron microscopy by the manufacturer, the effective resolution of the microscope could be established. We found that a uniform resolution <25 nm in the focal plane was achieved for the highest power we used.

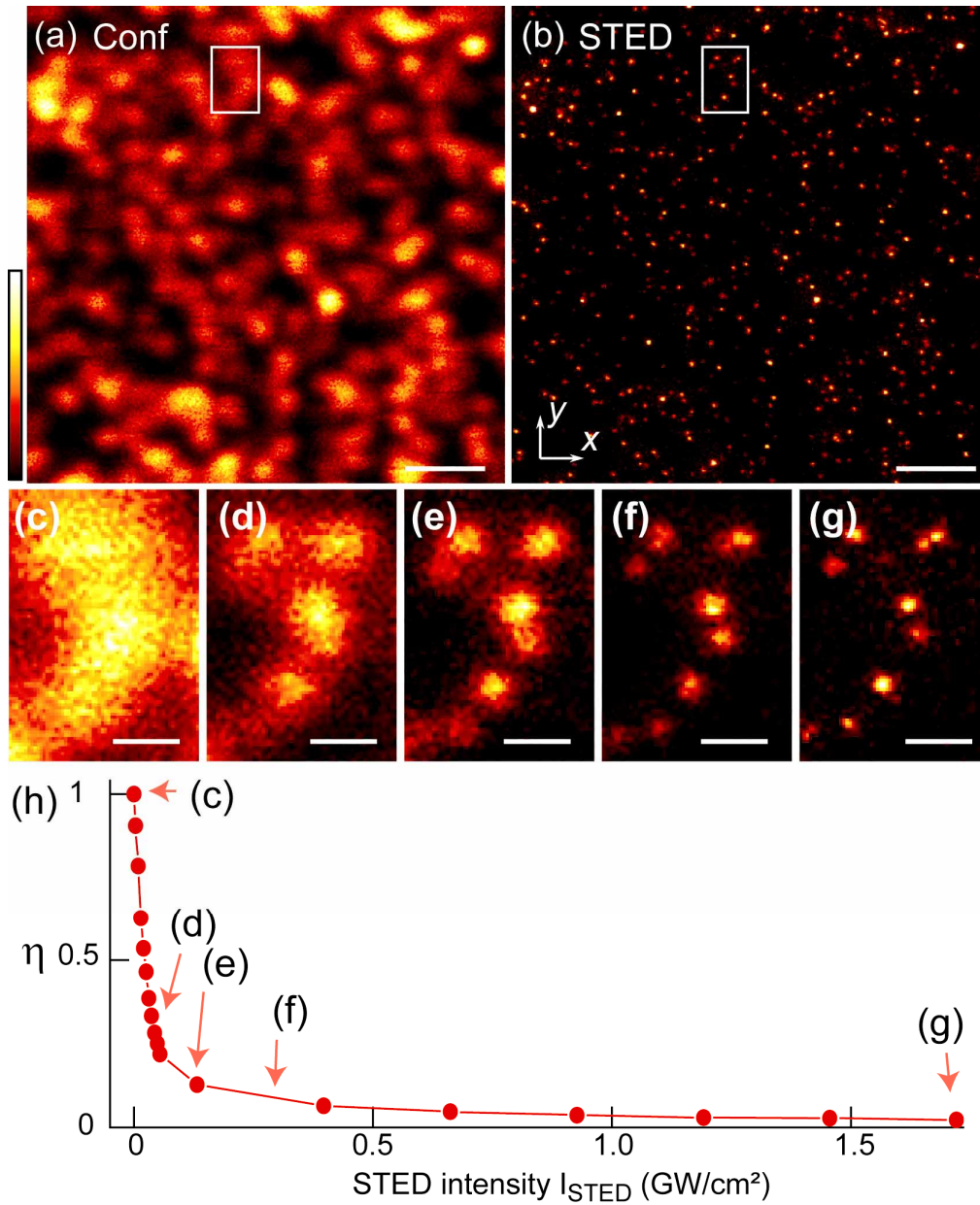


Fig. 2. Resolution enhancement realized by STED microscopy. (a,b) Confocal(a) and STED (b) image of 24 nm fluorescent beads on a cover slip. (c-g) The area of the white rectangle shown in (a) and (b) recorded with different STED intensities. The resolution gain can directly be observed. (h) STED depletion measured on the same sample. The intensity settings for the measurements (c-g) are marked by red arrows. Scale bar in (a,b) 1 μm , in (c-g) 200 nm. Images were recorded with a pixel size of 15 nm and then interpolated to a pixel size of 10 nm. Multimedia file movie 1(avi, 2.6 MB).

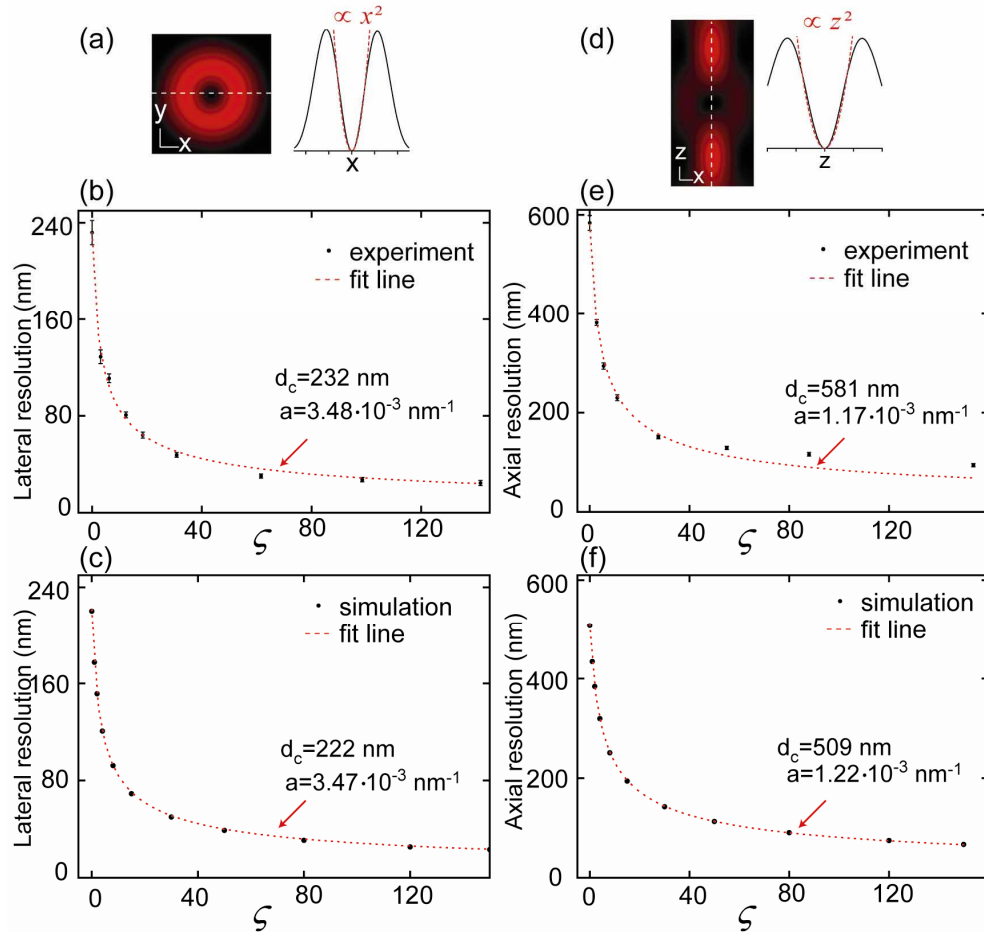


Fig. 3. Resolution dependence on the saturation factor for different depletion patterns.(a,d) Parabolic fit (red dashed line) to the depletion pattern for the lateral (a) and axial (d) direction. (b,e) Experimental data for lateral (b) and axial (e) confinements. Note the small error bars. (c,f) The simulated values for the lateral (c) and axial (f) resolution for different saturation factors. For both the simulated and experimental values an excellent match to the square root dependence (red dotted line) is observed.

Combining the information from the resolution measurements and the depletion curve allowed for the examination of the dependence of the measured resolution on the applied saturation factor. The use of an ensemble measurement avoids the problems associated with the imaging of isolated single molecules. Figure 3(b) shows that the measured lateral resolution values match closely with the fitted curve for the inverse square root law in Eq. (7). The result of the fitting process gives a value of $a = 0.00348 \text{ nm}^{-1}$. To demonstrate the generality of the law derived we examined the depletion pattern created for optimum axial confinement [18]. Figure 3(e) shows the dependence of the resolution on the saturation factor for this second configuration. The square root fit also matches this experimental data for $a = 0.00117 \text{ nm}^{-1}$. The deviation of the fit at high saturation factors can be partially ascribed to the random distribution of the beads. This non-uniformity makes it difficult to ensure the exact coincidence of the centres of the imaged beads with the imaging plane in the experiment.

Separately, *ab-initio* calculations of the effective PSF were undertaken. Only the physical parameters of the setup and the measured fluorescence suppression curve were utilized. Measurements of PSFs on gold nanobeads indicated a smaller than nominal effective NA of the objective lens. We therefore assumed $\text{NA}=1.36$ throughout our calculations. The dependence of the resolution obtained from the simulations is shown in Fig. 3(c) and (f). The

values of a are found to be 0.00347 nm^{-1} and 0.00122 nm^{-1} for the lateral and axial confinements, respectively. The agreement of the absolute values with our experiments is very good indicating little or no aberrations in the depletion beam. For the confocal FWHM we find larger experimental than theoretical values, especially along the optic axis. This is typical for aberrations in the excitation and detection pathways. Their influence becomes negligible for larger saturation values. The close and independent match of the square root law with both the experimental and ab-initio data underscores the validity of Eq. (7). Further, the distinct factors a and I_s allow us to separate the effects of the form of the depletion pattern from that of the spectroscopic properties of the dye system employed.

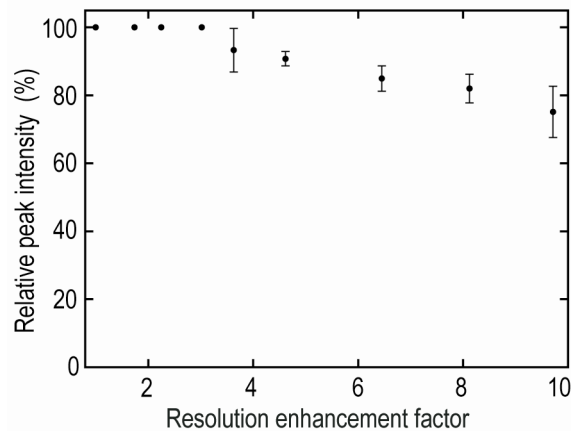


Fig. 4. Relative peak intensity of the STED image versus the factor of resolution enhancement in comparison to a confocal microscope. The value of 100 % implies that the fluorescence from the doughnut centre keeps the same value as without the STED beam. With larger resolution enhancement factors, the non-zero central minimum of the doughnut reduces the desired fluorescence signal from the doughnut centre. Nonetheless, even for a factor of 10 resolution increase in all directions in the focal plane, the percentage of photons discarded by STED is < 25 %.

A noteworthy aspect of the use of the polymer phase plate is the high quality of the resultant depletion doughnut. An important parameter characterising the quality of a doughnut is the depth of the minimum in the centre of the doughnut. The value of the minimum influences the remaining peak intensity. In the ideal case of a zero intensity minimum no signal reduction in the STED image is expected when imaging features much smaller than the PSF. For a non-zero value of the local minimum the peak intensity in the STED image is suppressed with respect to the corresponding confocal one, resulting in a reduced brightness. The relative peak intensity was evaluated by measuring the peak height of 13-17 isolated beads and comparing it to the geometric mean of the corresponding confocal values before and after the STED measurement in order to account for photobleaching. The dependence of the peak intensity on resolution enhancement factor relative to a confocal microscope is shown in Fig. 4. The data shown was corrected to account for the influence of the finite bead size on the peak intensity. An enhancement factor of ~ 10 in the two lateral directions is accompanied by a resulting peak intensity of ~ 75 %. This corresponds to a depth of the central minimum of about 0.3 % relative to the maximum of the depletion pattern. Importantly, for an enhancement factor of 4 in the lateral directions, typical for many biological applications, nearly no reduction in peak intensity is observed, meaning that STED does not discard fluorescence photons that contribute to the information gain. Even for a lateral resolution improvement by an order of magnitude in the focal plane, the loss of fluorescence photons is smaller than 25 % of the total number of photons that would be registered without STED from the subdiffraction area probed.

The ability to resolve features well below the diffraction limit is evidenced by the imaging of a densely packed colloidal crystal nanostructure. 200 nm spheres were organized on a hexagonal lattice by confined convective assembly [23, 24] and imaged. Due to the brightness of the object, confocal and STED images were recorded with four avalanche photodiodes counting the stream of fluorescence photons in parallel. The dead times at high count rates (> 1 MHz) were considered as specified by the manufacturer. While the confocal image, shown in Fig. 5(a), allows us to observe line defects, it yields only a blur in the defect free regions, as pictured in the inset. The STED image, in contrast, is able to reproduce the nanostructure with a high degree of fidelity.

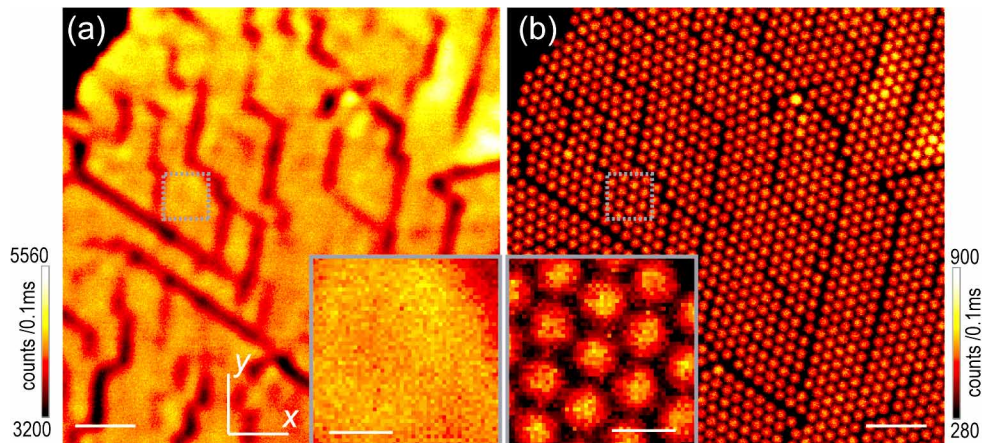


Fig. 5. Imaging of 200 nm self assembled colloids: (a) confocal image with the STED counterpart. (b). Scale bar 1 μ m, in insets scale bar 250 nm (movie2, avi, 2.8 MB). All images are raw data.

5. Summary and outlook

We have demonstrated that knowledge of two parameters, the saturation intensity and the depletion pattern steepness is sufficient to reliably predict the resolution of a STED microscope for a wide range of STED intensities using a very simple formula. It is relevant to note that the setup used employs readily available off the shelf components, including an inexpensive polymer phase plate for making the doughnut. The use of this phase plate has been shown to result in an increased brightness, and a uniform effective resolution in the lateral dimension. The demonstrated ability to perform STED with diode lasers [25] including CW lasers [22], along with the described implementation as a reference will make the method more accessible to a diverse set of disciplines, thereby allowing them to more easily enjoy the benefits of this 'diffraction-unlimited' far-field imaging technique.

Acknowledgments

This work was supported by the Alexander von Humboldt Foundation (CKU). We would like to thank Gael Moneron for helpful discussion about the two phase plates and also W. Kluge and the optics workshop for preparing the axial phase plate. Furthermore, many thanks to Lars Kastrup for useful suggestions.